Frontiers of Information Technology & Electronic Engineering
www.jzus.zju.edu.cn; engineering.cae.cn; www.springerlink.com
ISSN 2095-9184 (print); ISSN 2095-9230 (online)
E-mail: jzus@zju.edu.cn

Three-dimensional localization of near-field and strictly noncircular sources using steering vector decomposition*

Zheng LI[†1,2], Jinqing SHEN[1,2], Xiaofei ZHANG[†‡1,2]

[1]*College of Electronic and Information Engineering, Nanjing University of Aeronautics and Astronautics, Nanjing 211106, China*

[2]*Key Laboratory of Dynamic Cognitive System of Electromagnetic Spectrum Space, Ministry of Industry and Information Technology, Nanjing 211106, China*

[†]E-mail: lizhengjsnj@163.com; zhangxiaofei@nuaa.edu.cn

Received Jan. 19, 2021; Revision accepted June 6, 2021; Crosschecked Jan. 28, 2022

Abstract: The three-dimensional localization problem for noncircular sources in near-field with a centro-symmetric cross array is rarely studied. In this paper, we propose an algorithm with improved estimation performance. We decompose the multiple parameters of the steering vector in a specific order so that it can be converted into the products of several matrices, and each of the matrices includes only one parameter. On this basis, each parameter to be resolved can be estimated by performing a one-dimensional spatial spectral search. Although the computational complexity of the proposed algorithm is several times that of our previous algorithm, the estimation performance, including its error and resolution, with respect to the direction of arrival, is improved, and the range estimation performance can be maintained. The superiority of the proposed algorithm is verified by simulation results.

Key words: Localization; Centro-symmetric cross array; Noncircular sources; Near-field; Steering vector decomposition
https://doi.org/10.1631/FITEE.2100034 **CLC number:** TN911.7

1 Introduction

Unlike the wavefronts of far-field (FF) sources, those of near-field (NF) sources are assumed to be spherical rather than planar (Swindlehurst and Kailath, 1988). Consequently, the direction of arrival (DOA) algorithms for FF sources are not applicable to NF sources. Besides DOA information, the range information for NF sources also needs to be obtained; i.e., it is a problem not only for direction finding, but also for localization (Swindlehurst and Kailath, 1988; Van Trees, 2002). In DOA estimation, signals with noncircularity, e.g., amplitude modulated (AM) or binary phase shift keying (BPSK) modulated signals (Chargé et al., 2001; Haardt and Romer, 2004), have been widely studied because the noncircularity property can be exploited to enhance estimation performance (Chargé et al., 2001; Abeida and Delmas, 2006; Steinwandt et al., 2014, 2016; Zheng et al., 2017).

Some researchers have considered the localization problem for NF and noncircular (NC) sources (Xie et al., 2015a, 2015b; Chen et al., 2018; Shu et al., 2021). However, because the array configurations used in these papers are linear, the problem considered is actually two-dimensional localization. Studies of the three-dimensional (3D) localization problem for NF and NC sources with a centro-symmetric cross array (CSCA) have been reported very rarely. Although

‡ Corresponding author
* Project supported by the National Natural Science Foundation of China (Nos. 61971217, 61971218, 61631020, and 61601167)
ORCID: Zheng LI, https://orcid.org/0000-0002-0050-7026; Xiaofei ZHANG, https://orcid.org/0000-0003-1464-1987

some studies used the same configuration, the source type was restricted to non-Gaussian sources (Challa and Shamsunder, 1996; Wu and Yan, 2020). What is more, the source in our study is NC, which means that there is one more parameter, i.e., the NC phase. Consequently, the existing methods are not directly applicable. Recently, we proposed an algorithm using connection-matrices (CMs) for this problem (Li et al., 2021). This algorithm is able to obtain satisfactory estimation performance while avoiding the multi-dimensional spatial spectral search.

In this study, to further improve the estimation performance for the same problem, we propose an algorithm that decomposes the multiple parameters of the steering vector in a specific order so that it can be converted into the products of several matrices, and each of the matrices includes only one parameter. On this basis, each parameter to be resolved can be estimated by performing a one-dimensional (1D) spatial spectral search. Although the computational complexity of the proposed algorithm is several times that of our previous algorithm using CMs, simulation results have confirmed that it can obtain better angle estimation performance, including error and resolution, while maintaining the range estimation performance. Note that the proposed algorithm does not need additional angle-pairing.

Notations: Bold upper- and lower-case letters denote matrices and vectors, respectively; $(\cdot)^{\mathrm{T}}$ and $(\cdot)^{\mathrm{H}}$ denote the transpose and conjugate transpose operators, respectively; $(\cdot)^{+}$ and $(\cdot)^{-1}$ denote the pseudo-inverse and inverse operators, respectively; $\otimes$ denotes the Kronecker product; $\det(\cdot)$ and $\mathrm{diag}(\cdot)$ denote the determinant calculation and diagonal operator, respectively; $\boldsymbol{I}_m$ denotes the $m\times m$ identity matrix.

2 Data model

Fig. 1 shows the CSCA configuration. CSCA consists of two symmetric uniform linear arrays (ULAs) that are orthogonal and intersectant. Both ULAs, including $2M+1$ sensors, are assumed to be located on the x- and y-axis, and the distance between adjacent sensors is within $\lambda/4$ (Grosicki et al., 2005), where λ is the wavelength. The intersection of CSCA is the central sensor of the two ULAs, and is regarded as the reference sensor. All the sources are considered to be in the Fresnel region, i.e., $0.62(D^3/\lambda)^{0.5}<r_k<2D^2/\lambda$ (Hoole, 2001), where D denotes the aperture of the array, and r_k denotes the range between the k^{th} source and the reference sensor, $k=1, 2, \cdots, K$. The angle-pair of the k^{th} source is (θ_k, ϕ_k) or (α_k, β_k), where $\theta_k\in(0, 90°)$, $\phi_k\in(-180°, 180°)$, $\alpha_k, \beta_k\in(0, 180°)$, $\cos^2\alpha_k+\cos^2\beta_k<1$, and $d\le\lambda/4$.

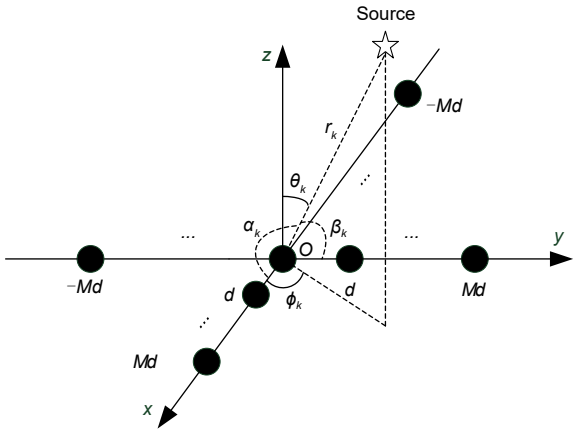

Fig. 1 The centro-symmetric cross array configuration

Assume that CSCA receives K signals located in the Fresnel region with zero-mean. All the signals are uncorrelated, narrow-band, and strictly NC. K is known and $K\le 2M$. Under these assumptions, the signals received from the x- and y-axis are (Gan et al., 2008; Steinwandt et al., 2014)

$$\boldsymbol{x}(t)=\boldsymbol{A}_x\boldsymbol{s}(t)+\boldsymbol{n}_x(t)=\boldsymbol{A}_x\boldsymbol{\phi}\boldsymbol{s}_0(t)+\boldsymbol{n}_x(t), \quad (1)$$

$$\boldsymbol{y}(t)=\boldsymbol{A}_y\boldsymbol{s}(t)+\boldsymbol{n}_y(t)=\boldsymbol{A}_y\boldsymbol{\phi}\boldsymbol{s}_0(t)+\boldsymbol{n}_y(t), \quad (2)$$

where $\boldsymbol{s}(t)=\boldsymbol{f}\boldsymbol{s}_0(t)$ denotes the signal vector and $\boldsymbol{s}_0(t)\in\mathbb{R}^K$, $\boldsymbol{\phi}=\mathrm{diag}\left(\mathrm{e}^{\mathrm{j}\varphi_1},\mathrm{e}^{\mathrm{j}\varphi_2},\cdots,\mathrm{e}^{\mathrm{j}\varphi_K}\right)$, and φ_k ($k=1, 2, \cdots, K$) denotes the NC phase of the k^{th} source. $\boldsymbol{A}_x=[\boldsymbol{a}_x(v_1, r_1), \boldsymbol{a}_x(v_2, r_2), \cdots, \boldsymbol{a}_x(v_K, r_K)]$ and $\boldsymbol{A}_y=[\boldsymbol{a}_y(u_1, r_1), \boldsymbol{a}_y(u_2, r_2), \cdots, \boldsymbol{a}_y(u_K, r_K)]$ are the steering matrices with $u_k=\sin\theta_k\sin\phi_k$ and $v_k=\sin\theta_k\cos\phi_k$. $\boldsymbol{n}_x(t)$ and $\boldsymbol{n}_y(t)$ are the additive white Gaussian noises. The steering vectors $\boldsymbol{a}_x(v_k, r_k)$, $\boldsymbol{a}_y(u_k, r_k)$ of $\boldsymbol{A}_x$ and $\boldsymbol{A}_y$ are expressed as (Challa and Shamsunder, 1996)

$$\boldsymbol{a}_x(v_k,r_k)=[\mathrm{e}^{\mathrm{j}(-M\omega_{xk}+M^2\eta_{xk})},\cdots,\mathrm{e}^{\mathrm{j}(-\omega_{xk}+\eta_{xk})},1,\mathrm{e}^{\mathrm{j}(\omega_{xk}+\eta_{xk})},\cdots,\mathrm{e}^{\mathrm{j}(M\omega_{xk}+M^2\eta_{xk})}]^{\mathrm{T}}, \quad (3)$$

$$\begin{aligned}\boldsymbol{a}_y(u_k,r_k)=[&\mathrm{e}^{\mathrm{j}(-M\omega_{yk}+M^2\eta_{yk})},\cdots,\mathrm{e}^{\mathrm{j}(-\omega_{yk}+\eta_{yk})},\\&1,\mathrm{e}^{\mathrm{j}(\omega_{yk}+\eta_{yk})},\cdots,\mathrm{e}^{\mathrm{j}(M\omega_{yk}+M^2\eta_{yk})}]^{\mathrm{T}},\end{aligned}\tag{4}$$

where $\omega_{xk}=-2\pi dv_k/\lambda$, $\omega_{yk}=-2\pi du_k/\lambda$, $\eta_{xk}=\pi d^2(1-v_k^2)/(\lambda r_k)$, $\eta_{yk}=\pi d^2(1-u_k^2)/(\lambda r_k)$, and $k=1, 2, \cdots, K$. Note that $\cos\alpha_k=v_k$ and $\cos\beta_k=u_k$.

3 The proposed algorithm

3.1 Steering vector decomposition

We firstly stack $\boldsymbol{x}(t)$, $\boldsymbol{y}(t)$, and their conjugations to construct the extended received signal as (Li et al., 2021)

$$\begin{aligned}\boldsymbol{z}(t)&=\begin{bmatrix}\boldsymbol{x}(t)\\\boldsymbol{x}^*(t)\\\boldsymbol{y}(t)\\\boldsymbol{y}^*(t)\end{bmatrix}=\begin{bmatrix}\boldsymbol{A}_x\boldsymbol{\phi}\\\boldsymbol{A}_x^*\boldsymbol{\phi}^*\\\boldsymbol{A}_y\boldsymbol{\phi}\\\boldsymbol{A}_y^*\boldsymbol{\phi}^*\end{bmatrix}\boldsymbol{s}_0(t)+\begin{bmatrix}\boldsymbol{n}_x(t)\\\boldsymbol{n}_x^*(t)\\\boldsymbol{n}_y(t)\\\boldsymbol{n}_y^*(t)\end{bmatrix}\\&=\boldsymbol{B}\boldsymbol{s}_0(t)+\boldsymbol{n}'(t),\end{aligned}\tag{5}$$

where

$$\begin{aligned}\boldsymbol{B}&=\left[(\boldsymbol{A}_x\boldsymbol{\phi})^{\mathrm{T}},(\boldsymbol{A}_x^*\boldsymbol{\phi}^*)^{\mathrm{T}},(\boldsymbol{A}_y\boldsymbol{\phi})^{\mathrm{T}},(\boldsymbol{A}_y^*\boldsymbol{\phi}^*)^{\mathrm{T}}\right]^{\mathrm{T}}\\&=[\boldsymbol{b}(\alpha_1,\beta_1,r_1,\varphi_1),\boldsymbol{b}(\alpha_2,\beta_2,r_2,\varphi_2),\cdots,\\&\quad\boldsymbol{b}(\alpha_K,\beta_K,r_K,\varphi_K)],\end{aligned}\tag{6}$$

$$\boldsymbol{b}(\alpha_k,\beta_k,r_k,\varphi_k)=\begin{bmatrix}\boldsymbol{a}_x(\alpha_k,r_k)\mathrm{e}^{\mathrm{j}\varphi_k}\\\boldsymbol{a}_x^*(\alpha_k,r_k)\mathrm{e}^{-\mathrm{j}\varphi_k}\\\boldsymbol{a}_y(\beta_k,r_k)\mathrm{e}^{\mathrm{j}\varphi_k}\\\boldsymbol{a}_y^*(\beta_k,r_k)\mathrm{e}^{-\mathrm{j}\varphi_k}\end{bmatrix}\tag{7}$$

denote the extended steering matrix and steering vector, respectively. Note that we decompose $\boldsymbol{a}_x(\alpha_k,r_k)\mathrm{e}^{\mathrm{j}\varphi_k}$ and $\boldsymbol{a}_y(\beta_k,r_k)\mathrm{e}^{\mathrm{j}\varphi_k}$ in a special order as

$$\boldsymbol{a}_x(\alpha_k,r_k)=\boldsymbol{C}_x(\alpha_k)\boldsymbol{h}_x(r_k)\cdot 1\cdot 1,\tag{8}$$

$$\boldsymbol{a}_x(\alpha_k,r_k)=\boldsymbol{I}_{2M+1}\boldsymbol{I}_{2M+1}\boldsymbol{C}_x(\alpha_k)\boldsymbol{h}_x(r_k),\tag{9}$$

$$\boldsymbol{a}_y(\beta_k,r_k)=\boldsymbol{C}_y(\beta_k)\boldsymbol{h}_y(r_k)\cdot 1\cdot 1,\tag{10}$$

$$\boldsymbol{a}_y(\beta_k,r_k)=\boldsymbol{I}_{2M+1}\boldsymbol{I}_{2M+1}\boldsymbol{C}_y(\beta_k)\boldsymbol{h}_y(r_k),\tag{11}$$

where

$$\boldsymbol{C}_x(\alpha_k)=\begin{bmatrix}\mathrm{e}^{\mathrm{j}(-M\omega_{xk})}&&&&\\&\ddots&&&\\&&\mathrm{e}^{\mathrm{j}(-\omega_{xk})}&&\\&&&1&\\&&&\mathrm{e}^{\mathrm{j}(\omega_{xk})}&\\&&\iddots&&\\\mathrm{e}^{\mathrm{j}(M\omega_{xk})}&&&&\end{bmatrix},\tag{12}$$

$$\boldsymbol{C}_y(\beta_k)=\begin{bmatrix}\mathrm{e}^{\mathrm{j}(-M\omega_{yk})}&&&&\\&\ddots&&&\\&&\mathrm{e}^{\mathrm{j}(-\omega_{yk})}&&\\&&&1&\\&&&\mathrm{e}^{\mathrm{j}(\omega_{yk})}&\\&&\iddots&&\\\mathrm{e}^{\mathrm{j}(M\omega_{yk})}&&&&\end{bmatrix},\tag{13}$$

$$\boldsymbol{h}_x(r_k)=[\mathrm{e}^{\mathrm{j}(M^2\eta_{xk})},\cdots,\mathrm{e}^{\mathrm{j}(\eta_{xk})},1]^{\mathrm{T}},\tag{14}$$

$$\boldsymbol{h}_y(r_k)=[\mathrm{e}^{\mathrm{j}(M^2\eta_{yk})},\cdots,\mathrm{e}^{\mathrm{j}(\eta_{yk})},1]^{\mathrm{T}}.\tag{15}$$

According to Eqs. (8)–(11), we can rewrite $\boldsymbol{b}(\alpha_k, \beta_k, r_k, \varphi_k)$ as

$$\begin{aligned}&\boldsymbol{b}(\alpha_k,\beta_k,r_k,\varphi_k)\\&=\boldsymbol{Q}_1(\alpha_k)\boldsymbol{Q}_2(r_k)\boldsymbol{Q}_3(\beta_k)\boldsymbol{Q}_4(r_k)\boldsymbol{p}(\varphi_k),\end{aligned}\tag{16}$$

where

$$\boldsymbol{Q}_1(\alpha_k)=\mathrm{diag}\left(\boldsymbol{C}_x(\alpha_k),\boldsymbol{C}_x^*(\alpha_k),\boldsymbol{I}_{2M+1},\boldsymbol{I}_{2M+1}\right),\tag{17}$$

$$\boldsymbol{Q}_2(r_k)=\mathrm{diag}\left(\boldsymbol{h}_x(r_k),\boldsymbol{h}_x^*(r_k),\boldsymbol{I}_{2M+1},\boldsymbol{I}_{2M+1}\right),\tag{18}$$

$$\boldsymbol{Q}_3(\beta_k)=\mathrm{diag}\left(1,1,\boldsymbol{C}_y(\beta_k),\boldsymbol{C}_y^*(\beta_k)\right),\tag{19}$$

$$\boldsymbol{Q}_4(r_k)=\mathrm{diag}\left(1,1,\boldsymbol{h}_y(r_k),\boldsymbol{h}_y^*(r_k)\right),\tag{20}$$

and

$$\begin{aligned}&\boldsymbol{b}(\alpha_k,\beta_k,r_k,\varphi_k)\\&=\boldsymbol{Q}_5(\beta_k)\boldsymbol{Q}_6(r_k)\boldsymbol{Q}_7(\alpha_k)\boldsymbol{Q}_8(r_k)\boldsymbol{p}(\varphi_k),\end{aligned}\tag{21}$$

where

$$\boldsymbol{Q}_5(\beta_k)=\mathrm{diag}\left(\boldsymbol{I}_{2M+1},\boldsymbol{I}_{2M+1},\boldsymbol{C}_y(\beta_k),\boldsymbol{C}_y^*(\beta_k)\right),\tag{22}$$

$$\boldsymbol{Q}_6(r_k)=\mathrm{diag}\left(\boldsymbol{I}_{2M+1},\boldsymbol{I}_{2M+1},\boldsymbol{h}_y(r_k),\boldsymbol{h}_y^*(r_k)\right),\tag{23}$$

$$\boldsymbol{Q}_7(\alpha_k)=\mathrm{diag}\left(\boldsymbol{C}_x(\alpha_k),\boldsymbol{C}_x^*(\alpha_k),1,1\right),\tag{24}$$

$$\boldsymbol{Q}_8(r_k)=\mathrm{diag}\left(\boldsymbol{h}_x(r_k),\boldsymbol{h}_x^*(r_k),1,1\right),\tag{25}$$

$$\boldsymbol{p}(\varphi_k)=[\mathrm{e}^{\mathrm{j}\varphi_k},\mathrm{e}^{-\mathrm{j}\varphi_k},\mathrm{e}^{\mathrm{j}\varphi_k},\mathrm{e}^{-\mathrm{j}\varphi_k}]^{\mathrm{T}}.\tag{26}$$

Eqs. (16) and (21) show that the multiple parameters in the steering vector can be decomposed into different matrices so that each matrix has only one parameter.

3.2 Initial estimation for α_k

We obtain an estimation of the covariance matrix of $\boldsymbol{z}(t)$ from

$$\hat{\boldsymbol{R}}=\frac{1}{J}\sum_{t=1}^{J}\boldsymbol{z}(t)\boldsymbol{z}^{\mathrm{H}}(t), \tag{27}$$

where J denotes the number of snapshots. Then we perform eigenvalue decomposition (EVD) on $\hat{\boldsymbol{R}}$ as

$$\hat{\boldsymbol{R}}=\hat{\boldsymbol{E}}_{\mathrm{s}}\hat{\boldsymbol{D}}_{\mathrm{s}}\hat{\boldsymbol{E}}_{\mathrm{s}}^{\mathrm{H}}+\hat{\boldsymbol{E}}_{\mathrm{n}}\hat{\boldsymbol{D}}_{\mathrm{n}}\hat{\boldsymbol{E}}_{\mathrm{n}}^{\mathrm{H}}, \tag{28}$$

to obtain the noise subspace $\hat{\boldsymbol{E}}_{\mathrm{n}}$, composed of the $8M+4-K$ minimum eigenvalues of $\hat{\boldsymbol{R}}$, and have

$$\begin{aligned}&\boldsymbol{b}^{\mathrm{H}}(\alpha_k,\beta_k,r_k,\varphi_k)\hat{\boldsymbol{E}}_{\mathrm{n}}\hat{\boldsymbol{E}}_{\mathrm{n}}^{\mathrm{H}}\boldsymbol{b}(\alpha_k,\beta_k,r_k,\varphi_k)=0,\\&k=1,2,\cdots,K,\end{aligned} \tag{29}$$

due to the multiple signal classification principle (Schmidt, 1986). According to Eq. (16), Eq. (29) can be rewritten as

$$\begin{aligned}&(\boldsymbol{Q}_1\boldsymbol{Q}_2\boldsymbol{Q}_3\boldsymbol{Q}_4\boldsymbol{p})^{\mathrm{H}}\hat{\boldsymbol{E}}_{\mathrm{n}}\hat{\boldsymbol{E}}_{\mathrm{n}}^{\mathrm{H}}(\boldsymbol{Q}_1\boldsymbol{Q}_2\boldsymbol{Q}_3\boldsymbol{Q}_4\boldsymbol{p})=0,\\&k=1,2,\cdots,K.\end{aligned} \tag{30}$$

Consequently, the rank-reduction (RARE) technique (Pesavento et al., 2001) can be combined to yield

$$\det\left(\left(\boldsymbol{Q}_1(\alpha_k)\right)^{\mathrm{H}}\hat{\boldsymbol{E}}_{\mathrm{n}}\hat{\boldsymbol{E}}_{\mathrm{n}}^{\mathrm{H}}\boldsymbol{Q}_1(\alpha_k)\right)=0,k=1,2,\cdots,K. \tag{31}$$

Then we find K maximum peaks of

$$f_1(\alpha)=\left(\det\left((\boldsymbol{Q}_1(\alpha))^{\mathrm{H}}\hat{\boldsymbol{E}}_{\mathrm{n}}\hat{\boldsymbol{E}}_{\mathrm{n}}^{\mathrm{H}}\boldsymbol{Q}_1(\alpha)\right)\right)^{-1}, \tag{32}$$

to obtain all coarse estimations $\hat{\alpha}_k^{\mathrm{c}}$ for α_k.

3.3 Estimation of r_k and β_k

We submit $\hat{\alpha}_k^{\mathrm{c}}$ into $\boldsymbol{Q}_1$. Then according to Eq. (29) and the RARE technique we have

$$\begin{aligned}&\det\left(\left(\boldsymbol{Q}_1(\hat{\alpha}_k^{\mathrm{c}})\boldsymbol{Q}_2(r_k)\right)^{\mathrm{H}}\hat{\boldsymbol{E}}_{\mathrm{n}}\hat{\boldsymbol{E}}_{\mathrm{n}}^{\mathrm{H}}\boldsymbol{Q}_1(\hat{\alpha}_k^{\mathrm{c}})\boldsymbol{Q}_2(r_k)\right)=0,\\&k=1,2,\cdots,K.\end{aligned} \tag{33}$$

Then we find the maximum peak of

$$\begin{aligned}f_2(r)=&\left(\det\left(\left(\boldsymbol{Q}_1(\hat{\alpha}_k^{\mathrm{c}})\boldsymbol{Q}_2(r)\right)^{\mathrm{H}}\right.\right.\\&\left.\left.\cdot\hat{\boldsymbol{E}}_{\mathrm{n}}\hat{\boldsymbol{E}}_{\mathrm{n}}^{\mathrm{H}}\boldsymbol{Q}_1(\hat{\alpha}_k^{\mathrm{c}})\boldsymbol{Q}_2(r)\right)\right)^{-1},\ k=1,2,\cdots,K,\end{aligned} \tag{34}$$

to obtain each $\hat{r}_k$. Note that $\hat{\alpha}_k^{\mathrm{c}}$ and $\hat{r}_k$ are auto-paired with each other. Then we submit the paired $(\hat{\alpha}_k^{\mathrm{c}},\hat{r}_k)$ into $\boldsymbol{Q}_1$ and $\boldsymbol{Q}_2$ to yield

$$\begin{aligned}&\det\left(\left(\boldsymbol{Q}_1(\hat{\alpha}_k^{\mathrm{c}})\boldsymbol{Q}_2(\hat{r}_k)\boldsymbol{Q}_3(\beta_k)\right)^{\mathrm{H}}\hat{\boldsymbol{E}}_{\mathrm{n}}\hat{\boldsymbol{E}}_{\mathrm{n}}^{\mathrm{H}}\boldsymbol{Q}_1(\hat{\alpha}_k^{\mathrm{c}})\right.\\&\left.\cdot\boldsymbol{Q}_2(\hat{r}_k)\boldsymbol{Q}_3(\beta_k)\right)=0,\ k=1,2,\cdots,K.\end{aligned} \tag{35}$$

Similar to $\hat{r}_k$, we find the maximum peak of

$$\begin{aligned}f_3(\beta)=&\left(\det\left(\left(\boldsymbol{Q}_1(\hat{\alpha}_k^{\mathrm{c}})\boldsymbol{Q}_2(\hat{r}_k)\boldsymbol{Q}_3(\beta)\right)^{\mathrm{H}}\hat{\boldsymbol{E}}_{\mathrm{n}}\right.\right.\\&\left.\left.\cdot\hat{\boldsymbol{E}}_{\mathrm{n}}^{\mathrm{H}}\boldsymbol{Q}_1(\hat{\alpha}_k^{\mathrm{c}})\boldsymbol{Q}_2(\hat{r}_k)\boldsymbol{Q}_3(\beta)\right)\right)^{-1},\ k=1,2,\cdots,K,\end{aligned} \tag{36}$$

to obtain each $\hat{\beta}_k$. Note that $\hat{\alpha}_k^{\mathrm{c}}$, $\hat{r}_k$, and $\hat{\beta}_k$ are auto-paired with each other; i.e., K pairs of $(\hat{\alpha}_k^{\mathrm{c}},\hat{r}_k,\hat{\beta}_k)$ have been obtained.

3.4 Final estimation of α_k

According to Eq. (21), Eq. (29) can be rewritten as

$$\begin{aligned}&(\boldsymbol{Q}_5\boldsymbol{Q}_6\boldsymbol{Q}_7\boldsymbol{Q}_8\boldsymbol{h})^{\mathrm{H}}\hat{\boldsymbol{E}}_{\mathrm{n}}\hat{\boldsymbol{E}}_{\mathrm{n}}^{\mathrm{H}}(\boldsymbol{Q}_5\boldsymbol{Q}_6\boldsymbol{Q}_7\boldsymbol{Q}_8\boldsymbol{h})=0,\\&k=1,2,\cdots,K.\end{aligned} \tag{37}$$

Similar to Eq. (31), we have

$$\begin{aligned}&\det\left(\left(\boldsymbol{Q}_5(\beta)\boldsymbol{Q}_6(r)\boldsymbol{Q}_7(\alpha)\right)^{\mathrm{H}}\hat{\boldsymbol{E}}_{\mathrm{n}}\hat{\boldsymbol{E}}_{\mathrm{n}}^{\mathrm{H}}\boldsymbol{Q}_5(\beta)\right.\\&\left.\cdot\boldsymbol{Q}_6(r)\boldsymbol{Q}_7(\alpha)\right)=0,k=1,2,\cdots,K.\end{aligned} \tag{38}$$

Because we have obtained K pairs of $(\hat{\alpha}_k^{\mathrm{c}},\hat{r}_k,\hat{\beta}_k)$, we submit $(\hat{\alpha}_k^{\mathrm{c}},\hat{r}_k,\hat{\beta}_k)$ into Eq. (38) and perform a 1D partial spatial spectral search to finally obtain a precise estimation of $\hat{\alpha}_k$ as

$$\begin{aligned}\hat{\alpha}_k=&\arg_{\alpha}\max_{\alpha\in[\hat{\alpha}_k^{\mathrm{c}}-\Delta,\hat{\alpha}_k^{\mathrm{c}}+\Delta]}\left(\det\left(\left(\boldsymbol{Q}_5(\hat{\beta}_k)\boldsymbol{Q}_6(\hat{r}_k)\boldsymbol{Q}_7(\hat{\alpha}_k^{\mathrm{c}})\right)^{\mathrm{H}}\right.\right.\\&\left.\left.\cdot\hat{\boldsymbol{E}}_{\mathrm{n}}\hat{\boldsymbol{E}}_{\mathrm{n}}^{\mathrm{H}}\boldsymbol{Q}_5(\hat{\beta}_k)\boldsymbol{Q}_6(\hat{r}_k)\boldsymbol{Q}_7(\hat{\alpha}_k^{\mathrm{c}})\right)\right)^{-1},k=1,2,\cdots,K,\end{aligned} \tag{39}$$

where Δ denotes the partial search scope. After performing Eq. (39), $(\hat{\alpha}_k, \hat{\beta}_k, \hat{r}_k)$ are obtained.

3.5 Procedure of the algorithm

We summarize the procedure of the proposed algorithm as follows:

Step 1: Calculate the covariance matrix $\boldsymbol{R}$ of $\boldsymbol{z}(t)$ in Eq. (5) and perform EVD for $\boldsymbol{R}$ to yield the noise subspace matrix $\hat{\boldsymbol{E}}_{\mathrm{n}}$ as Eq. (28).

Step 2: Perform 1D global spatial spectral search once to find $\hat{\alpha}_k^{\mathrm{c}}$ corresponding to the K maximum peaks of $f_1(\alpha)$ in Eq. (32).

Step 3: Submit $\hat{\alpha}_k^{\mathrm{c}}$ into $\boldsymbol{Q}_1$ and perform 1D global spatial spectral search according to Eq. (34) K times to find $\hat{r}_k$ such that each corresponds to the maximum peak of $f_2(r)$ in Eq. (34) and is paired with $\hat{\alpha}_k^{\mathrm{c}}$.

Step 4: Submit $(\hat{\alpha}_k^{\mathrm{c}}, \hat{r}_k)$ into $\boldsymbol{Q}_1$ and $\boldsymbol{Q}_2$, and perform a 1D global spatial spectral search according to Eq. (36) K times to find $\hat{\beta}_k$ such that each corresponds to the maximum peak of $f_3(\beta)$ in Eq. (36) and is paired with $(\hat{\alpha}_k^{\mathrm{c}}, \hat{r}_k)$.

Step 5: Submit $(\hat{\alpha}_k^{\mathrm{c}}, \hat{r}_k, \hat{\beta}_k)$ into $\boldsymbol{Q}_5$, $\boldsymbol{Q}_6$, and $\boldsymbol{Q}_7$, and perform a 1D partial spatial spectral search K times to obtain the final estimation of $\hat{\alpha}_k$ from Eq. (39).

4 Complexity analysis

In this paper, the complexity is characterized by complex multiplications. For the proposed algorithm, calculating $\hat{\boldsymbol{R}}$ requires $O[(8M+4)^2 J]$. Operating EVD for $\hat{\boldsymbol{R}}$ requires $O[(8M+4)^3]$. Estimating $\hat{\alpha}_k^{\mathrm{c}}$ requires $O\{(180/d_s)[(6M+4)^3+(8M+4-K)(6M+4)(14M+8)]\}$. Estimating $\hat{r}_k$ paired with $\hat{\alpha}_k^{\mathrm{c}}$ requires $O\{K[(2M^2-0.62(2M^3)^{0.5})/d_r][(4M+4)^3+(8M+4-K)(6M+4)(14M+8)]\}$. Estimating $\hat{\beta}_k$ paired with $(\hat{\alpha}_k^{\mathrm{c}}, \hat{r}_k)$ requires $O\{K(180/d_s)[(2M+4)^3+(8M+4-K)(72M^2+128M+48)]\}$. Estimating $\hat{\alpha}_k$ paired with $(\hat{r}_k, \hat{\beta}_k)$ requires $O\{(2K\Delta/d_s)[(2M+4)^3+(8M+4-K)(72M^2+128M+48)]\}$.

Fig. 2 shows a comparison of the computational complexity between different algorithms versus M, where J=300, K=3, d_{s}=0.01°, and d_{r}=0.01λ. d_{s} and d_{r} are the search steps for angles and range, respectively. The complexity of the proposed algorithm is several times that of the previous algorithm, but the proposed algorithm has better performance in terms of angle estimation precision and resolution. This superiority is demonstrated in the next section.

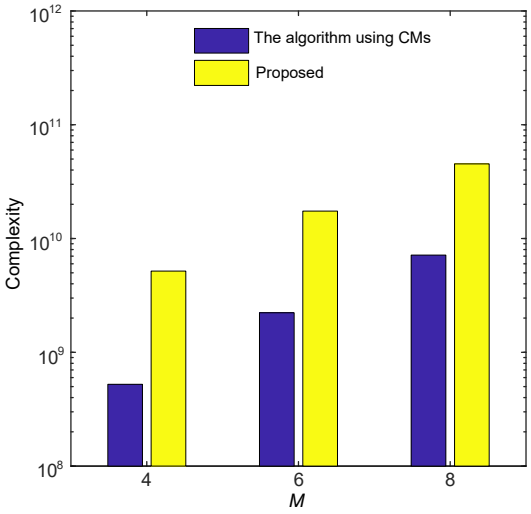

Fig. 2 The computational complexity versus M

5 Simulation results

The Cramer-Rao bound (CRB) in this section was provided by Li et al. (2021). The root mean square error (RMSE) is defined as

$$\mathrm{RMSE}_{(\alpha,\beta)} = \frac{1}{K}\sum_{k=1}^{K}\sqrt{\frac{1}{C}\sum_{c=1}^{C}\left(\left(\hat{\alpha}_{k,c}-\alpha_k\right)^2+\left(\hat{\beta}_{k,c}-\beta_k\right)^2\right)}, \quad (40)$$

$$\mathrm{RMSE}_{\alpha} = \frac{1}{K}\sum_{k=1}^{K}\sqrt{\frac{1}{C}\sum_{c=1}^{C}\left(\hat{\alpha}_{k,c}-\alpha_k\right)^2}, \quad (41)$$

$$\mathrm{RMSE}_{\beta} = \frac{1}{K}\sum_{k=1}^{K}\sqrt{\frac{1}{C}\sum_{c=1}^{C}\left(\hat{\beta}_{k,c}-\beta_k\right)^2}, \quad (42)$$

$$\mathrm{RMSE}_{r} = \frac{1}{K}\sum_{k=1}^{K}\sqrt{\frac{1}{C}\sum_{c=1}^{C}\left(\hat{r}_{k,c}-r_k\right)^2}, \quad (43)$$

where C is the number of Monte-Carlo trials, $\hat{\alpha}_{k,c}$, $\hat{\beta}_{k,c}$, and $\hat{r}_{k,c}$ denote the estimates for α_k, β_k, and r_k in the c^{th} trial, respectively. In this section, we set C=300 and d=0.25λ.

Simulation 1 Figs. 3 and 4 show the scatter plots of angle–angle and angle–range. We supposed that M=5, K=2, (α_1, β_1, r_1, φ_1)=(70°, 75°, 2.5λ, 10°), (α_2, β_2, r_2, φ_2)=(80°, 85°, 3.5λ, 20°), d_{s}=0.01°, d_{r}=0.01λ, and J=200. The signal-to-noise ratio (SNR) was set

to 10 and 15 dB. Figs. 3 and 4 clearly show that the proposed algorithm was effective regarding both angle–angle and angle–range in all 300 trials. Note that the algorithm using CMs needs angle-pairing, while the proposed algorithm does not. Consequently, theoretically the proposed algorithm does not suffer from the pairing error.

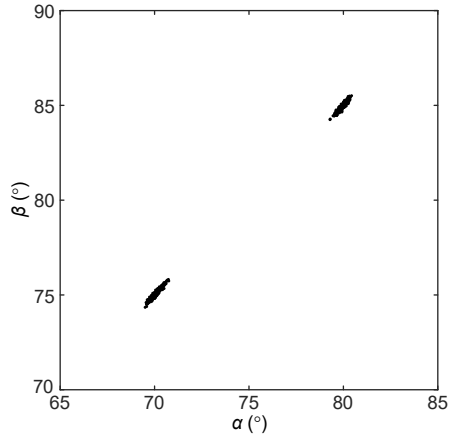

Fig. 3 Scatter plot of angle–angle

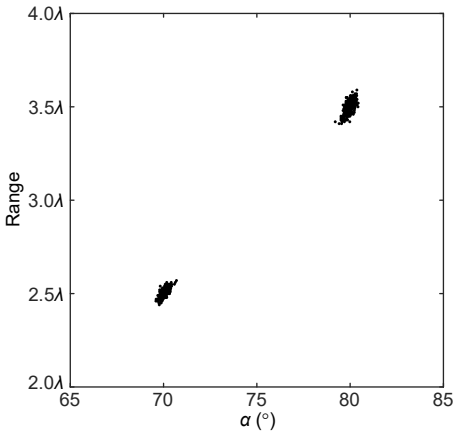

Fig. 4 Scatter plot of angle–range

Simulation 2 In this simulation, we compared the RMSE performance of the initial and final estimations of the proposed algorithm for α_k versus SNR, where M=5, K=2, $(\alpha_1, \beta_1, r_1, \varphi_1)$=(80°, 80°, 3$\lambda$, 10°), $(\alpha_2, \beta_2, r_2, \varphi_2)$=(100°, 100°, 5$\lambda$, 20°), Δ=2°, d_s=0.01°, d_r=0.01λ, and J=400 in Fig. 5 and SNR=10 dB in Fig. 6. From these simulations, we found that the final estimation can yield more precise results than the initial estimation, which reveals the necessity of the final estimation. A possible explanation is that the initial estimation is performed without any information about β_k and r_k, while before performing the final estimation, $\hat{\beta}_k$ and $\hat{r}_k$ have been obtained, and this information is exploited in the final estimation.

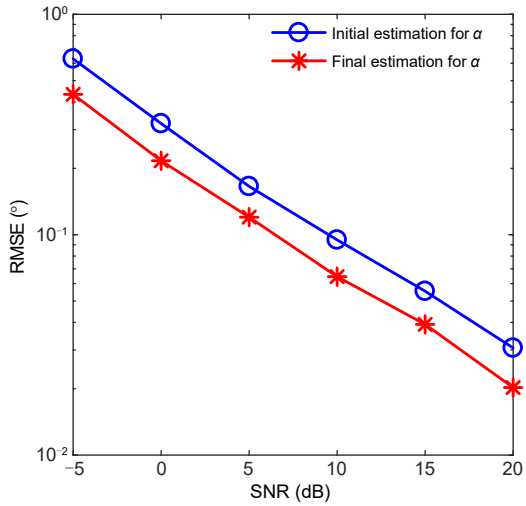

Fig. 5 The accuracy of the initial and final estimations of the proposed algorithm for α_k versus SNR

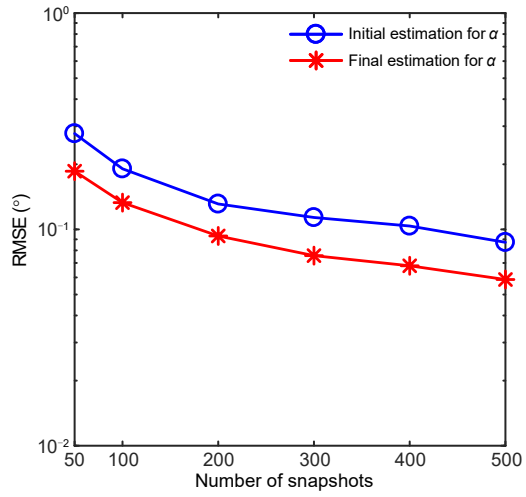

Fig. 6 The accuracy of the initial and final estimations of the proposed algorithm for α_k versus the number of snapshots

Simulation 3 In this simulation, we compared the RMSE performance of different algorithms versus SNR. All parameters were identical to those in Fig. 5. Figs. 7 and 8 show that the proposed algorithm outperformed the algorithm using CMs in terms of the DOA estimation error, while the two algorithms had very similar range estimation errors. This indicates that the range estimation performance of the proposed algorithm can be maintained.

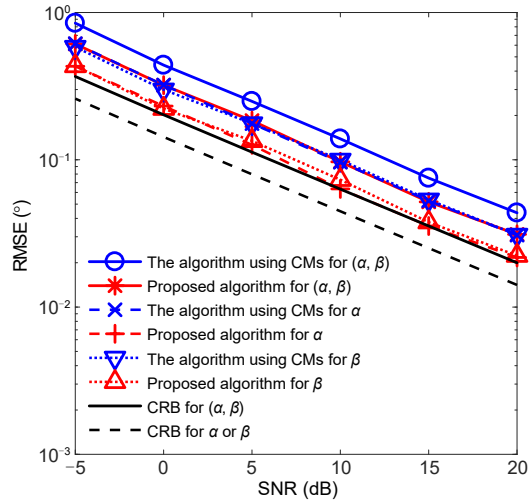

Fig. 7 The RMSE results regarding DOA estimation versus SNR

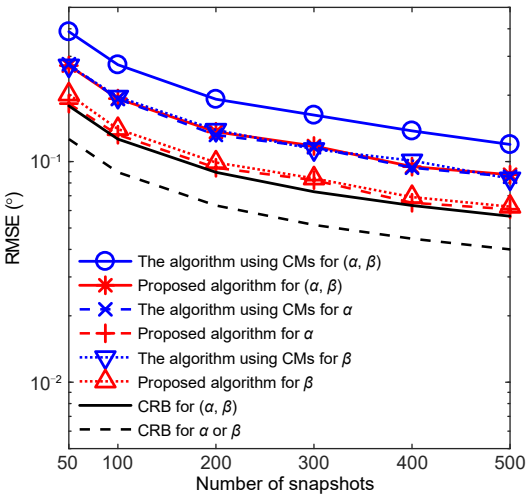

Fig. 9 The RMSE results regarding DOA estimation versus the number of snapshots

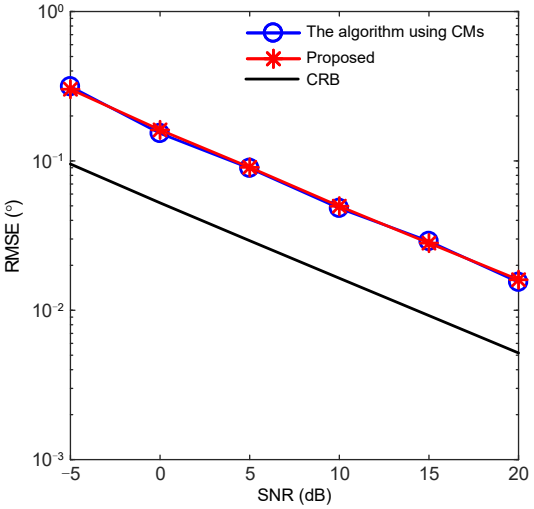

Fig. 8 The RMSE results regarding range estimation versus SNR

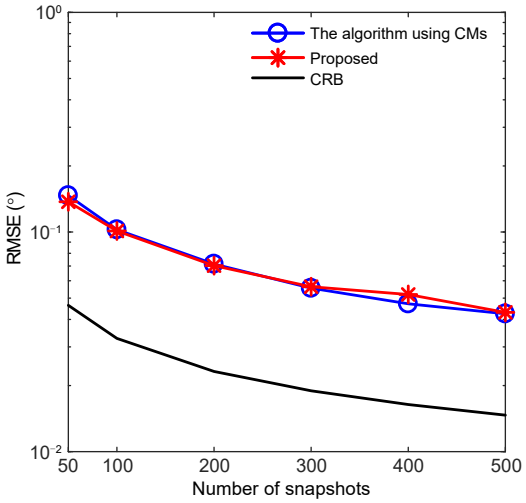

Fig. 10 The RMSE results regarding range estimation versus the number of snapshots

Simulation 4 In this simulation, we compared the RMSE performance of different algorithms versus the number of snapshots, where SNR=10 dB. All parameters were identical to those in Fig. 6. Similar to Figs. 7 and 8, Figs. 9 and 10 show the improvement in performance of the proposed algorithm for DOA estimation, and the similar performance for range estimation compared with the algorithm using CMs.

Simulation 5 Figs. 11 and 12 illustrate the DOA resolution performance of different algorithms versus angle and range separation for two sources with close angle and close range, respectively. In Fig. 11, M=5, SNR=20 dB, J=500, d_s=0.01°, d_r=0.001λ, (α_1, β_1, r_1, φ_1)=(80°, 80°, 3λ, 10°), (α_2, β_2, r_2, φ_2)=(80°+Δ_α, 80°+Δ_α, 3.5λ, 10°+Δ_α), and in Fig. 12, M=6, (α_1, β_1, r_1, φ_1)=(80°, 80°, 3λ, 10°), (α_2, β_2, r_2, φ_2)=(81°, 81°, 3λ+Δ_r, 11°). Other parameters were identical to those in Fig. 11, where Δ_α and Δ_r respectively denote angle and range separation. The two sources were considered to be successfully resolved if $|\hat{\alpha}_k - \alpha_k| < |\alpha_2 - \alpha_1|/2$, $|\hat{\beta}_k - \beta_k| < |\beta_2 - \beta_1|/2$, or $|\hat{r}_k - r_k| < |r_2 - r_1|/2$, where k=1, 2. Figs. 11 and 12 show that the probability of successful recognition for the proposed algorithm was obviously higher than that of the algorithm using CMs. This indicates that the proposed algorithm has better DOA resolution for sources with close angle or close range.

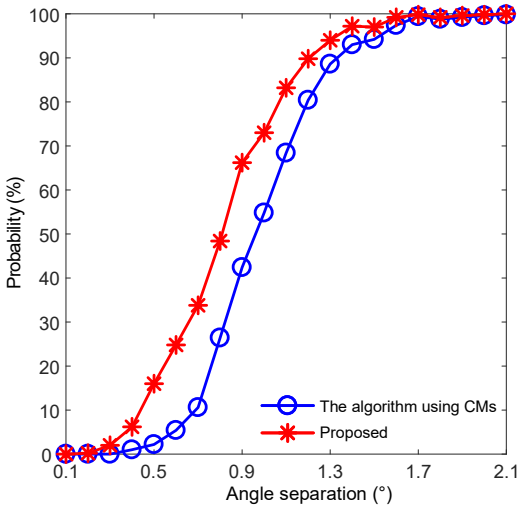

Fig. 11 The DOA resolution versus angle separation

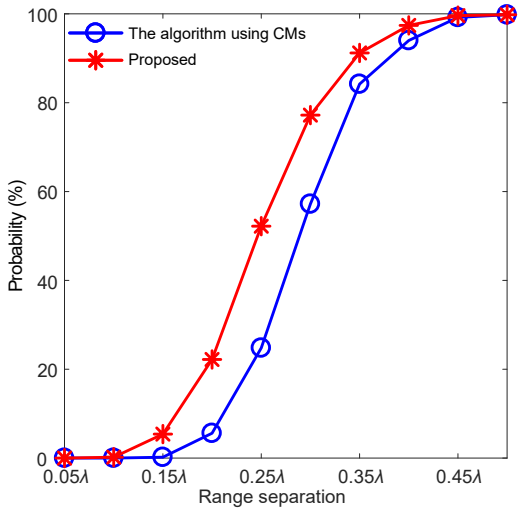

Fig. 12 The DOA resolution versus range separation

6 Conclusions

The 3D localization algorithm proposed in this study is for NF and strictly second-order NC sources with CSCA. The algorithm decomposes the multiple parameters of the steering vector in a specific order so that it can be converted into the products of several matrices, and each of the matrices includes only one parameter. On this basis, each parameter to be resolved can be estimated by performing a 1D spatial spectral search. Although the computational complexity of the proposed algorithm is several times that of our previous algorithm using CMs, its estimation performance, including estimation error and resolution, with respect to DOA, is better than that of the algorithm using CMs, while the range estimation performances of the two algorithms are very close.

Contributors

Zheng LI designed the research and processed the data. Zheng LI and Jinqing SHEN drafted the paper. Xiaofei ZHANG helped organize the paper. Zheng LI, Jinqing SHEN, and Xiaofei ZHANG revised and finalized the paper.

Compliance with ethics guidelines

Zheng LI, Jinqing SHEN, and Xiaofei ZHANG declare that they have no conflict of interest.

References

Abeida H, Delmas JP, 2006. MUSIC-like estimation of direction of arrival for noncircular sources. *IEEE Trans Signal Process*, 54(7):2678-2690. https://doi.org/10.1109/TSP.2006.873505

Challa RN, Shamsunder S, 1996. 3-D spherical localization of multiple non-Gaussian sources using cumulants. Proc 8th Workshop on Statistical Signal and Array Processing, p.101-104. https://doi.org/10.1109/SSAP.1996.534830

Chargé P, Wang Y, Saillard J, 2001. A non-circular sources direction finding method using polynomial rooting. *Signal Process*, 81(8):1765-1770. https://doi.org/10.1016/S0165-1684(01)00071-8

Chen H, Liu W, Zhu WP, et al., 2018. Noncircularity-based localization for mixed near-field and far-field sources with unknown mutual coupling. IEEE Int Conf on Acoustics, Speech and Signal Processing, p.3236-3240. https://doi.org/10.1109/ICASSP.2018.8462266

Gan L, Gu JF, Wei P, 2008. Estimation of 2-D DOA for noncircular sources using simultaneous SVD technique. *IEEE Antenn Wirel Propag Lett*, 7:385-388. https://doi.org/10.1109/LAWP.2008.2000875

Grosicki E, Abed-Meraim K, Hua YB, 2005. A weighted linear prediction method for near-field source localization. *IEEE Trans Signal Process*, 53(10):3651-3660. https://doi.org/10.1109/TSP.2005.855100

Haardt M, Romer F, 2004. Enhancements of unitary ESPRIT for non-circular sources. IEEE Int Conf on Acoustics, Speech, and Signal Processing, p.ii101-ii104. https://doi.org/10.1109/ICASSP.2004.1326204

Hoole PR, 2001. Smart Antennas and Signal Processing: for Communications, Biomedical and Radar Systems. WIT Press, Southampton, UK.

Li Z, Shen J Q, Zhai H, et al., 2021. 3-D localization for near-field and strictly noncircular sources via centro-symmetric cross array. *IEEE Sens J*, 21(6):8432-8440. https://doi.org/10.1109/JSEN.2020.3048713

Pesavento M, Gershman AB, Wong KM, 2001. Direction of arrival estimation in partly calibrated time-varying sensor arrays. Proc IEEE Int Conf on Acoustics, Speech, and Signal Processing, p.3005-3008. https://doi.org/10.1109/ICASSP.2001.940282

Schmidt R, 1986. Multiple emitter location and signal parameter

estimation. *IEEE Trans Antenn Propag*, 34(3):276-280. https://doi.org/10.1109/TAP.1986.1143830

Shu T, Li LN, He J, 2021. Near-field localization for non-circular sources in the presence of sensor phase uncertainties. *IEEE Wirel Commun Lett*, 10(3):562-566. https://doi.org/10.1109/LWC.2020.3037917

Steinwandt J, Roemer F, Haardt M, et al., 2014. R-dimensional ESPRIT-type algorithms for strictly second-order non-circular sources and their performance analysis. *IEEE Trans Signal Process*, 62(18):4824-4838. https://doi.org/10.1109/TSP.2014.2342673

Steinwandt J, Roemer F, Haardt M, et al., 2016. Deterministic Cramér-Rao bound for strictly non-circular sources and analytical analysis of the achievable gains. *IEEE Trans Signal Process*, 64(17):4417-4431. https://doi.org/10.1109/TSP.2016.2566603

Swindlehurst AL, Kailath T, 1988. Passive direction-of-arrival and range estimation for near-field sources. Proc Annual 4th ASSP Workshop on Spectrum Estimation and Modeling, p.123-128. https://doi.org/10.1109/SPECT.1988.206176

Van Trees HL, 2002. Optimum Array Processing, Part IV of Detection, Estimation, and Modulation Theory. Wiley, New York, NY, USA.

Wu XH, Yan J, 2020. 3-D mixed far-field and near-field sources localization with cross array. *IEEE Trans Veh Technol*, 69(6):6833-6837. https://doi.org/10.1109/TVT.2020.2985903

Xie J, Tao HH, Rao X, et al., 2015a. Efficient method of passive localization for near-field noncircular sources. *IEEE Antenn Wirel Propag Lett*, 14:1223-1226. https://doi.org/10.1109/LAWP.2015.2399534

Xie J, Tao HH, Rao X, et al., 2015b. Real-valued localisation algorithm for near-field non-circular sources. *Electron Lett*, 51(17):1330-1331. https://doi.org/10.1049/el.2015.0454

Zheng W, Zhang XF, Sun HP, et al., 2017. Non-circular generalised-ESPRIT algorithm for direction of arrival estimation. *IET Radar Sonar Navig*, 11(5):736-744. https://doi.org/10.1049/iet-rsn.2016.0349